Journal of Membrane Science 373 (2011) 178–188

Contents lists available at ScienceDirect

Journal of Membrane Science

journal homepage: www.elsevier.com/locate/memsci

Modification and characterization of ultrafiltration membranes for treatment of produced water

Daniel Wandera [a], S. Ranil Wickramasinghe [b], Scott M. Husson [a,*]

[a] Department of Chemical and Biomolecular Engineering and Center for Advanced Engineering Fibers and Films, Clemson University, 127 Earle Hall, Clemson, SC 29634, USA
[b] Department of Chemical and Biological Engineering, Colorado State University, Fort Collins, CO 80523, USA

ARTICLE INFO

Article history:
Received 4 October 2010
Received in revised form 2 February 2011
Accepted 4 March 2011
Available online 12 March 2011

Keywords:
Antifouling
Impaired water
Sustainability
Temperature-responsive
Water treatment

ABSTRACT

This contribution describes the surface modification of low molecular weight cutoff regenerated cellulose ultrafiltration membranes by grafting poly(N-isopropylacrylamide) (PNIPAAm)-*block*-poly(oligoethylene glycol methacrylate) (PPEGMA) nanolayers from the membrane surface using surface-initiated atom transfer radical polymerization. The objective of the work was to change the membrane surface properties in ways that limit foulant accumulation on these membranes and provide an easy, chemical-free way to remove any attached foulants during produced water filtration. ATR-FTIR spectra confirmed the successful grafting of both polymers from the membrane surface. Analysis of AFM topographical images indicated that membrane surface roughness decreased slightly from 2.6 nm for the unmodified membrane to 1.7 nm following PNIPAAm-*b*-PPEGMA modification. The performance of the modified membranes was tested by measuring water flux using synthetic produced water developed from an oil-in-water emulsion. Polymer grafting led to a roughly 40% decrease in the water flux, but the final flux was comparable to commercial membranes used for removal of organics with high salt passage. Furthermore, modified membranes showed slower flux decline than unmodified membranes, and, hence, the modified membranes allowed a 13.8% higher cumulative volume of water to be processed over a 40 h cross-flow filtration run. To test potential for chemical-free cleaning, filtration runs were carried out before and after a temperature-controlled water rinse. Flux recovery was better for the modified membranes after a cold water rinse. The flux recovered fully to initial values for both the PNIPAAm- and PNIPAAm-*b*-PPEGMA-modified membranes; while only ~81% of the initial flux was recovered for the unmodified membrane. All three membranes exhibited poor salt rejection, as would be expected for ultrafiltration membranes. However, TOC removal efficiencies were higher than 97% for PNIPAAm-*b*-PPEGMA-modified membranes. Taken together, results from this work indicate that PNIPAAm-*b*-PPEGMA modified ultrafiltration membranes could be used to separate emulsified oils from large volumes of produced water at high flux.

© 2011 Elsevier B.V. All rights reserved.

1. Introduction

Produced water (PW) is oily water that is co-produced during oil and gas exploration and production. The volume of PW that is generated depends on how much is present in the reservoir as a natural water layer (formation water) and whether additional water is injected into the reservoir to force the oil to the surface. Increasing energy demands coupled with high oil and gas prices are driving the increased production of oil and gas from non-traditional sources such as tar sands, oil shale and coal bed methane (CBM) [1]. Here again, oil and gas production generates large volumes of PW, particularly from CBM wells, which contain many fractures and pores that can contain and transmit large volumes of water.

In the United States, PW accounted for 88% of the total volume of exploration and production material brought to the surface by the oil and gas industry in 2007. The total volume of PW generated from most of the nearly 1 million actively producing oil and gas wells in the United States in 2007 was estimated to be about 21 billion barrels (bbl) [2]. Khatib and Verbeek [3] reported that worldwide daily PW generation in 1999 was more than 210 million bbl which represents about 77 billion bbl of PW for the entire year, about three times the world oil production.

The volume of PW from conventional oil and gas wells does not remain constant, as the water-to-oil ratio increases over the lifetime of the well. For example, Khatib and Verbeck [3] reported that PW generated from several Shell operating units increased from 2.1 million bbl per day in 1990 to more than 6 million bbl per day in 2002. Clark and Veil [2] reported that US wells generated an average of more than 5 bbl of PW for each bbl of oil in 2007. For crude oil wells nearing the end of their productive

* Corresponding author. Tel.: +1 864 656 4502; fax: +1 864 656 0784.
E-mail address: shusson@clemson.edu (S.M. Husson).

0376-7388/$ – see front matter © 2011 Elsevier B.V. All rights reserved.
doi:10.1016/j.memsci.2011.03.010

lives, as much as 98% of the material brought to the surface can be PW. CBM wells, in contrast, produce a large volume of PW early in their life and the volume declines over time. For example, between 1999 and 2001, the volume of PW generated per well in the Powder River Basin dropped from 396 bbl per day to 177 bbl per day [4].

PW characteristics and physical properties vary considerably depending on the geographical location of the field, composition of the rocks surrounding the reservoir, the amount of time the rocks and water react and the origin of the water entering the reservoir. The total dissolved solids (TDS) ranges from 200 mg/L to 170,000 mg/L [5]. Recommended TDS for potable water is 500 mg/L and 1000–2000 mg/L for other beneficial uses such as stock ponds or irrigation. As a point of reference, average sea water has a TDS of 35,000 mg/L.

The proper management of PW is becoming a major issue for the public and regulators due to the high volumes generated and the disposal practices of many gas and oil companies. At the same time, oil and gas producing areas, especially for CBM, are located in arid areas of the United States where questions arise concerning the "wasting" of water through the generation and disposal of PW during production. Costs associated with PW management impact the profits of the oil and gas industry and potentially could halt production operations. In 2007, more than 98% of PW from onshore wells was injected underground with approximately 59% injected into producing formations to maintain formation pressure and increase output, while another 40% was injected into nonproducing formations for storage [2]. Injection of PW for storage in deep wells costs U.S. $0.50–$1.75 per bbl in wells that cost U.S. $400,000–$3,000,000 to install [6]. Four percent of the total PW (onshore and offshore) in 2007 was surface discharged after some pre-treatment, which can cause adverse effects to the environment [7]. Therefore, identifying and implementing appropriate beneficial uses for PW should provide overwhelming benefits for local communities and ecosystems and provide oil and gas companies with flexible, cost-saving water management options.

Conventional wastewater treatment technologies such as coagulation, flocculation, air flotation and gravity separation normally cannot meet the high purity requirements for discharge of PW [8]. There is a growing tendency to use membrane technology for PW treatment, and a number of studies have shown successful treatment of oily water using membranes [1,9–13]. Distinct advantages of membrane technology for treatment of PW include reduced sludge, high quality permeate and the possibility of total recycle water systems. These advantages, when considered along with the small space requirements, moderate capital costs, and ease of operation make membrane technology an economically competitive alternative or addition to traditional wastewater treatment technologies [10,13,14]. Although membranes can treat PW, their widespread use is hindered by a decline in permeate flux experienced as a result of fouling. The flux decline is due to the adsorption and accumulation of rejected oil, suspended solids and other components in PW on the membrane surface (external fouling) and in the membrane pores (internal fouling). Fouling can be irreversible or resistant to cleaning, hence making the original flux unrecoverable. Physical cleaning techniques including membrane relaxation (where filtration is paused) and membrane backwashing (where permeate is pumped in the reverse direction through the membrane) have been incorporated in most membrane process designs as standard operating strategies to limit fouling [15]. These techniques have been shown to be effective for dealing with reversible fouling; however, they are less effective at limiting irreversible fouling. In addition to physical cleaning strategies, different types of chemical cleaning have been recommended. However, the harsh treatment procedure can damage the membrane and shorten its life span.

In this article, we present an approach to control membrane fouling during filtration of PW and to provide a chemical-free strategy to reverse foulant accumulation. Commercial, regenerated cellulose (RC) ultrafiltration membranes were surface modified by growing block copolymer nanolayers from the membrane surfaces by surface-initiated atom transfer radical polymerization (ATRP). Our hypothesis is that by controlling both the chemical and environmentally responsive conformational properties of these polymer layers at the nano-scale, we will limit foulant accumulation on these membranes and provide an easy, chemical-free way to remove any attached foulants. During ATRP, only surface bound radicals are formed; therefore, no radicals are co-produced in solution. Hence, polymer chains grow from the surface only and no polymer is co-produced in solution. As a controllable chain growth technique, ATRP allows for control of chain molecular weight (nanolayer thickness) to avoid pore filling [16]. Polymerization can be stopped by removal of the membrane from solution and then restarted by placing the membrane back into solution and reinitiating polymer chains. The controlled nature of the polymerization ensures that a high percentage of polymer chains remain active for reinitiation. This feature makes ATRP highly attractive for preparing block copolymers [17–20]. Modification can be done within membrane modules normally used for water purification since it is activated by a solution-phase catalyst. Our group [16,21–25] and others [19,20,26–28] have used ATRP to graft polymers with controlled architectures from flat and porous membrane surfaces.

Membranes were modified by grafting poly(N-isopropylacrylamide) (PNIPAAm)-*block*-poly(oligoethylene glycol methacrylate) (PPEGMA) nanolayers from the membrane surfaces. PNIPAAm exhibits a lower critical solution temperature (LCST) at 32 °C, as first reported by Heskins and Guillet [29]. PNIPAAm chains hydrate to form a random coil structure below LCST and collapse to form a globular structure above LCST. Since its physical and chemical properties are controlled easily by changing the temperature, PNIPAAm is used widely to prepare temperature-responsive materials, including many examples with membranes [19,20,30]. Therefore, PNIPAAm was grafted from membrane surfaces to make them temperature responsive. Previous work by our group has shown that PPEGMA can be grafted by ATRP from polyamide nanofiltration membranes to improve their antifouling properties [22]. Therefore, PPEGMA was grafted as the second block from PNIPAAm-modified membrane surfaces to improve their antifouling properties.

In previous work [22], our group used surface-initiated ATRP to graft block copolymers from commercial polyamide thin-film nanofiltration membranes for produced water treatment. One problem that was identified was the significant decrease of flux to unacceptable values due to modification. In this work, we set out to overcome that problem by moving to a more "open" ultrafiltration base membrane. Modification of these UF membranes imparts responsive chemistry to the surface and maintains high flux. Using a more open membrane will allow optimization of water quality versus permeate flux. We also switched the base material to regenerated cellulose, which itself has good fouling resistance towards hydrophobic compounds.

Initial measurements were made to determine the thickness evolution of the PNIPAAm nanolayers and to show that PNIPAAm chains remain active for relatively long polymerization times, making it possible to use polymerization time to adjust the nanolayer thickness while preserving some fraction of chain ends for subsequent reinitiation to graft the PPEGMA block. These studies also demonstrated the responsive nature of the PNIPAAm nanolayers and quantified the degree of layer swelling for grafted PNIPAAm. Thereafter, PNIPAAm-*b*-PPEGMA was grafted by surface-initiated ATRP from regenerated cellulose UF membranes. ATR-FTIR and AFM were used to characterize changes in the surface chemical

functionality and roughness of membranes as a result of modification. Short- and long-term water flux measurements were done with synthetic produced water.

2. Experimental

2.1. Materials

Commercial, composite ultrafiltration membranes with a nominal molecular weight cut-off (MWCO) of 5 kDa (Hydrosart, 14429-47, 47 mm dia.) were purchased from Sartorius Stedim Biotech. Commercial, composite UF membranes with a nominal MWCO of 1000 kDa (PLCXK) were provided by Millipore Corporation. These membranes comprise a thin regenerated cellulose layer on a polypropylene support.

Single-sided polished silicon wafers (1 cm × 3 cm) were used as substrates for studying the kinetics of PNIPAAm polymerization. These were purchased from Silicon Quest International.

The following chemicals were purchased from Sigma–Aldrich and used as received unless stated otherwise: azobisisobutyronitrile (AIBN, 98%), benzene (>99.5%), 2,2′-bipyridyl (>99%), 2-bromoisobutyryl bromide (2-BIB, 98%), 2-bromo-2-methylpropionic acid (BPA, 98%), copper(I) chloride (CuCl, >99.995%), copper(II) chloride ($CuCl_2$, 99.99%), glycidyl methacrylate (GMA, 95%), hydrogen peroxide (50% in water, ACROS), neutral aluminum oxide (~150 mesh, 58 Å), sodium chloride (NaCl, >99%), sulfuric acid (96% in water, ACROS), tris(2-dimethylaminoethyl)amine (Me_6TREN, >98%, ATRP Solutions, Inc.). HPLC grade solvents were purchased from Fisher Scientific, and these included chloroform, methanol, methyl ethyl ketone (MEK), n-hexane, water, and tetrahydrofuran (THF, anhydrous). Soybean oil (SO255) was purchased from Spectrum Chemicals.

Poly(ethylene glycol) methacrylate (PEGMA) macromonomer ($M_n \approx 360$ g/mol) containing monomethyl ether hydroquinone (650 ppm) inhibitor was purchased from Sigma–Aldrich. The inhibitor was removed before use by passing the PEGMA through a column of neutral aluminum oxide. N-isopropylacrylamide (NIPAAm, 97%) was purchased from Sigma–Aldrich and purified prior to use by dissolving it in benzene and then re-crystallizing it from n-hexane.

Deionized (DI) water used for flux measurements was prepared by passing distilled water through a compact Milli-Q Integral water purification system (Millipore Corporation) that was equipped with a 0.22 μm Millipax® sterile filter.

2.2. Kinetic study of polymer nanolayer growth from silicon substrates

2.2.1. Preparation and activation of silicon substrates

Before use, the silicon wafers were cleaned in deionized water for 30 min using an ultrasonic bath for agitation. To ensure thorough cleaning, the deionized water was changed every 10 min. The clean wafers were then treated with a freshly prepared 3:1 (v/v) mixture of concentrated sulfuric acid and hydrogen peroxide (piranha solution, use with caution: highly reactive with organic compounds) for 1 h at 60 °C, rinsed thoroughly with deionized water and then dried using a stream of high-purity nitrogen.

Surface activation with ATRP initiator groups was done using a protocol described in detail previously [31]. Briefly, to begin the surface activation process, a reactive layer of poly(glycidyl methacrylate) (PGMA) was deposited on the cleaned silicon substrates by dip coating from a 0.1 wt.% PGMA solution in chloroform using a speed of 0.14 cm/s. The PGMA-coated silicon substrates were annealed for 30 min at 110 °C under vacuum (~500 Pa). ATRP initiation sites were incorporated into the PGMA layer by reaction with vapor-phase BPA at ~130 Pa and 110 °C for 18 h. The ATRP-activated silicon substrates were soaked in chloroform for 10 min, rinsed with chloroform three times, and dried using a stream of high-purity nitrogen.

2.2.2. Polymerization from activated silicon substrates

Surface-initiated ATRP of PNIPAAm was carried out from initiator groups on the activated silicon substrate. A typical polymerization solution comprised monomer, NIPAAm (50.0 mM, 94.0 mg), dissolved in a 4:1 (v/v) solvent mixture of HPLC water and methanol (16.7 mL). Other formulations were studied, and results are available in Supplemental Information. Before transferring the polymerization solution to a nitrogen atmosphere glove box, the solution was de-oxygenated by three cycles of freeze–pump–thaw. In the glove box, all components of the catalyst system were added to the de-oxygenated solution. Because the mass and volume amounts of catalyst components were small, we prepared one large volume of catalyst solution for a use with a number of samples. To improve the precision of volume measurements, we used syringes (Hamilton, Inc.) with range of 0–50 μL or 0–100 μL and a precision of ±1 μL. In the sections that follow, we give the mass or volume used per silicon substrate or membrane sample, along with the final solution concentration of each component. Components of the catalyst included activator, CuCl (0.50 mM, 0.83 mg), deactivator, $CuCl_2$ (0.10 mM, 0.22 mg), and ligand, Me_6TREN (1.2 mM, 5.5 μL). A previously activated silicon substrate was then placed in the solution to begin polymerization. PNIPAAm polymerization was carried out at room temperature for times up to 60 min. PNIPAAm-grafted silicon substrates were removed from the polymerization solution at fixed time intervals, thoroughly washed with methanol and HPLC water and then dried using a stream of nitrogen.

2.3. Membrane modification

Scheme 1 illustrates the three step procedure to modify a regenerated cellulose membrane with PNIPAAm-*b*-PPEGMA by surface-initiated ATRP. ATRP initiator molecules were attached to the membrane, and then surface-initiated ATRP was done to graft PNIPAAm chains from the initiator groups. PPEGMA was then grafted as the second polymer block by re-initiation of PNIPAAm chains.

2.3.1. Membrane activation

The membranes were immersed in methanol for 15 min to remove glycerin, which is used as a structural preservative for these membranes; rinsed thoroughly with HPLC water to remove methanol; and then equilibrated with THF. Membranes were removed from the THF, dried with a stream of nitrogen, and transferred into the glove box. Membrane activation (i.e., incorporation of ATRP initiator groups) was done according to Bhut et al. [21]. After activation, the membranes were removed from the solution, washed thoroughly with THF and HPLC water and stored in THF until polymerization.

2.3.2. Polymerization from activated membranes

Surface-initiated ATRP of PNIPAAm was carried out from initiator groups on the activated membrane surface. The polymerization formulation and protocol were the same as that used for silicon substrates. PNIPAAm polymerization was carried out at room temperature for 1 h. PNIPAAm-modified membranes were removed from the polymerization solution, thoroughly washed with methanol and HPLC water and stored in methanol.

For modification with block copolymer nanolayers, PPEGMA was grafted from the PNIPAAm-modified membranes. The polymerization solution comprised monomer, PEGMA (0.10 M, 1.6 mL) dissolved in a 4:1 (v/v) solvent mixture of HPLC water and methanol

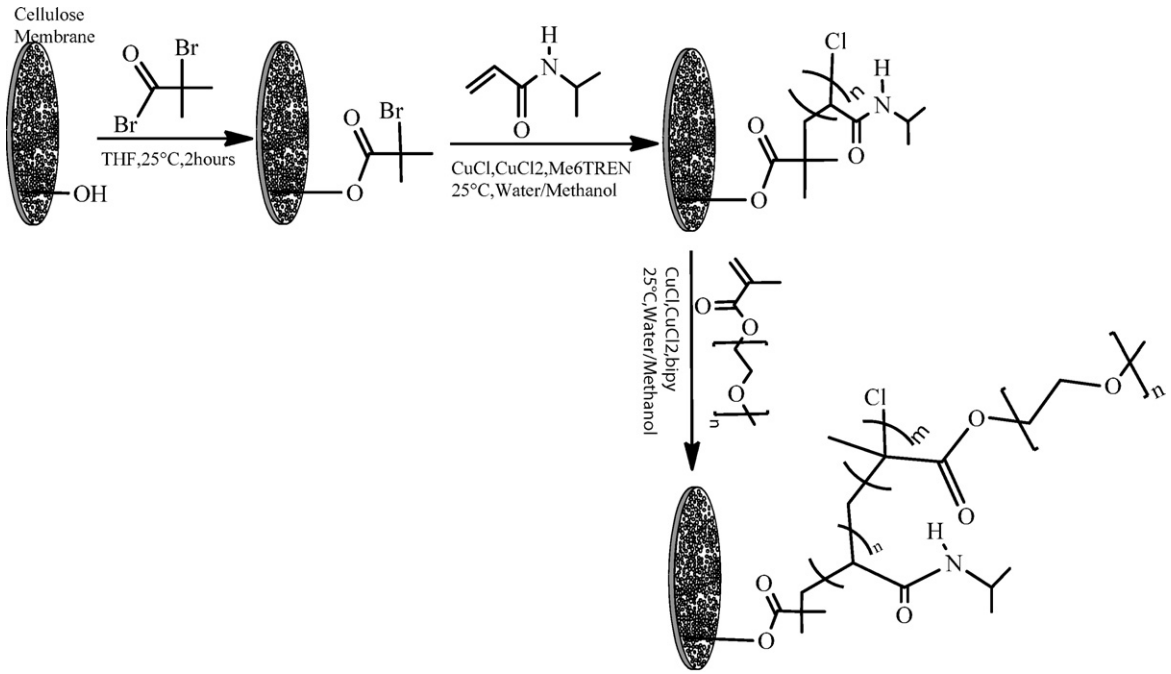

Scheme 1. Surface-initiated ATRP of PNIPAAm-*b*-PPEGMA from cellulose.

(50 mL). The solution was de-oxygenated and transferred to the glove box, where all components of the catalyst system were added. These included CuCl (0.50 mM), $CuCl_2$ (0.10 mM) and ligand, 2,2′-bipyridyl (1.2 mM). A PNIPAAm-modified membrane was removed from methanol, dried and placed into the solution to begin polymerization. PPEGMA polymerization was carried out at room temperature for 3 h. This protocol was followed based on previous work from our group on the surface-initiated growth of PPEGMA nanolayers at room temperature from silicon substrates [16]. From the silicon surfaces, the growth rates of PNIPAAm and PPEGMA were 54 and 0.48 nm/h, respectively. Thus, a 1 h PNIPAAm polymerization yields a layer thickness of about 54 nm, while a 3 h PPEGMA polymerization yields a layer thickness of about 1.4 nm. PNIPAAm-*b*-PPEGMA modified membranes were removed from the polymerization solution, thoroughly washed with methanol and HPLC water and stored in DI water.

2.4. Water flux measurements

A model, synthetic produced water was prepared to test the performance of pristine and modified membranes through flux measurements. The synthetic produced water was prepared by mixing soybean oil (5.44 mL), NaCl (500 mg), and DI water (1 L) and stirring the mixture with a magnetic stir bar (3/8 in. diameter, 2 in. length) in a 1 L flat-bottom Erlenmeyer flask at a constant speed of 600 rpm at 60 °C for 24 h. Soybean oil was used because it is commercially available with consistent properties. Experiments using soybean oil are therefore highly reproducible. Using the density of the soybean oil (0.919 g/mL) and the volume of soybean oil used (5.44 mL/L), we calculated the mass of dispersed oil in our synthetic model solution. Table 1 gives the characteristics of the model, synthetic produced water.

Water flux measurements were carried using 45 mm diameter membranes. A stirred ultrafiltration cell (model 8050, Millipore Corporation) was modified to increase the volumetric capacity to 300 mL by increasing the height of the cylinder. Membranes were loaded into the cell, which was filled with 300 mL of the synthetic produced water. The cell was connected to a nitrogen gas cylinder via high-pressure tubing. The system was placed on a magnetic stirring plate, which provided constant agitation at a speed of ~320 rpm during filtration. A constant pressure of 207 kPa was used for all of the experiments. The filtration cell was filled with fresh feed at 45 °C every 5 min to maintain a constant feed temperature during the course of the 60 min filtration experiment. We used warm (45 °C) PW because it is common for PW coming out of deep oil wells to be warm (above 40 °C). Permeate was collected in a beaker when the permeate outlet was opened, and the mass of permeate collected over time was measured using a balance. Permeate flux was calculated using Eq. (1), where M is the mass of permeate collected, ρ is the density, A is the effective membrane filtration area, and t is the time:

$$\text{Permeate flux} = \frac{M/P}{At} \quad (1)$$

The experimental procedure for the filtration experiments included carrying out a warm (45 °C) produced water filtration for 60 min, rinsing the membrane with cold (15 °C) DI water, and carrying out another warm produced water filtration for 30 min. Rinsing the membrane was done by filling the filtration cell containing the membrane with cold DI water and stirring for 5 min. The rinse solution was discarded from the cell, and the cell was filled again with warm produced water. This sequence of measurements was done to study the effectiveness of a cold water rinse at detaching any foulants that had accumulated on the membrane surface during the first filtration step. Control measurements were done with a warm water (45 °C) rinse.

Long-term cross-flow (CF) membrane filtration experiments using our model synthetic PW were carried out using a high

Table 1
Characteristics of model synthetic produced water.

Parameter	Value
Dispersed oil	5000 mg/L
Conductivity	1108 μs/cm
Total dissolved solids (TDS)	543 mg/L
Total organic carbon (TOC)	82.23 mg/L

pressure Septa® CF II medium/high foulant membrane cell system (GE Osmonics). The membrane cell system accommodates a 19 cm × 14 cm flat sheet membrane with an effective membrane area of 140 cm^2. The system was operated in recirculation mode using a Hydra-Cell pump (Wanner Engineering, Inc.). All experiments were carried out using a constant transmembrane pressure (TMP) and temperature of 414 kPa and 50 °C. The system was operated for at least 1 h before any permeate flux measurements were taken. Permeate flux values were calculated from the permeate volumes collected at different times.

2.5. Characterization

2.5.1. Ellipsometry

Multi-angle ellipsometry was used to measure the dry nanolayer (PNIPAAm) thickness on the silicon substrates as a function of polymerization time. Measurement and instrument details have been described elsewhere [31]. A refractive index of 1.525 was used for PGMA, 1.500 for BPA, 1.460 for PNIPAAm layers less than 50 nm thick and 1.470–1.490 for PNIPAAm layers greater than 50 nm thick [32]. Measurements were done at three locations for each sample and the data represent average values among the three measurements. In all cases, the coefficient of variance for the ellipsometric measurements was ≤3.5%.

Solvent-swollen layer thicknesses were measured as a function of temperature to analyze the temperature responsiveness of the grafted PNIPAAm layers. For these measurements, the silicon substrates were placed inside a specially designed cylindrical flow cell (Beaglehole Instruments) and contacted with solvent (water) at different temperatures supplied by a temperature-controlled bath. Data fitting was done using a fixed, temperature-dependent refractive index for the solvent and allowing the refractive index of the polymer nanolayer to vary. Both the refractive index of the nanolayer and its thickness were used as fitting parameters. Additional details of the flow cell and measurement procedure were given in the Supplemental Information of Samadi et al. [31].

2.5.2. ATR-FTIR

Attenuated total reflectance Fourier-transform infrared spectroscopy (ATR-FTIR) was used to characterize surface chemical properties of the unmodified, PNIPAAm-modified and PNIPAAm-*b*-PPEGMA-modified membranes. Spectra were obtained using a Thermo-Nicolet Magna 550 FTIR spectrometer equipped with a diamond ATR accessory. Measurements were done according to a procedure detailed elsewhere [24].

2.5.3. AFM

Atomic force microscopy (AFM) was used to characterize the changes in the surface topography and morphology of the silicon substrates and membranes resulting from surface modification. Images of the dry samples were obtained using a BioScope AFM (Veeco) with a NanoScope IIIA controller and a silicon cantilever (MikroMasch, NSC15/Si3N4/AIBS). Tapping mode AFM was done at a frequency of 1.0 Hz, and 256 scans were taken per image. Root-mean square (RMS) surface roughness of the 1.0 μm × 1.0 μm images was calculated using NanoScope software version 5.12. Three scans were done at three different places on the same 45 mm diameter membrane for unmodified and modified membranes. The standard deviation among roughness values was ±0.1 nm.

AFM images also were collected for PNIPAAm-modified silicon substrates in water at different temperatures using contact mode in order to analyze the temperature responsiveness of the grafted PNIPAAm layers.

2.6. Water quality analysis

2.6.1. Conductivity and TDS

The conductivity and total dissolved solids (TDS) concentration of the feed and permeate were measured using a multiple parameter SympHony™ meter (VWR). Salt concentrations were determined by measuring electrical conductivities and using a standard calibration; TDS was used as an indicator of the total amount of inorganic foulant material in the water.

2.6.2. TOC

Total organic carbon (TOC) concentrations of the feed and permeate were determined using a high temperature total organic carbon analyzer (Shimadzu TOC-V_{CSH}) that operates on a catalytic combustion method. Details about the instrument and operating conditions have been provided previously [33].

3. Results and discussion

3.1. Kinetics of surface-initiated ATRP of PNIPAAm

To study the thickness evolution of the grafted polymer nanolayers and to understand how different conditions influence polymer growth, a kinetic study of the surface-initiated ATRP of PNIPAAm was conducted using silicon substrates. Experiments were carried out for PNIPAAm only, as a kinetic study of surface-initiated ATRP of PPEGMA was conducted by our group previously [16]. Data from this part of the study were used to guide membrane modification work. The modified silicon surfaces were characterized by ellipsometry to measure nanolayer thickness versus polymerization time. AFM was used to determine changes in the surface topography and roughness of the silicon substrates. The reason silicon substrates were used is that ellipsometry cannot be used for direct measurements on the membranes.

Silicon substrates were activated by coating with PGMA and then functionalizing the PGMA with an ATRP initiator. This procedure was done to create a surface that mimics the three-dimensional nature of the membrane 'surface'. In a previous work from our group [25], it has been noted that PGMA on flat silicon substrates offers a more appropriate model than self-assembled monolayers for characterizing polymer growth kinetics, as it generates high initiator densities that better reflect the true nature of initiator incorporation within the membrane structure.

After annealing the PGMA-coated silicon substrates, the PGMA dry layer thicknesses were measured to be 6.0 ± 0.2 nm. The uncertainty represents the standard deviation in thickness among multiple locations on the silicon substrate surfaces. After incorporation of initiator groups, the dry layer thicknesses increased to 9.0 ± 0.5 nm. This increase in thickness indicates clearly that mass was added to the layer. Using the difference in these values, we estimated the density of initiator sites to be 15 ± 2 initiator molecules per nm^2.

Fig. 1 shows the increase in PNIPAAm dry layer thickness as a function of time following surface-initiated ATRP. These results show that the rate of PNIPAAm growth increased with increasing monomer concentration from 0.01 M to 0.05 M, which is a characteristic of surface-initiated ATRP.

A well-documented characteristic of controlled, surface-initiated ATRP from a low surface area substrate is a linear relationship between polymer layer thickness and time. As seen in Fig. 1, our polymerization protocol did not yield well-controlled growth. We conducted a control study in which fresh catalyst was added to the polymerization system once the layer thickness reached a plateau value. No additional growth was observed; hence, we attribute the nonlinear growth to chain termination and not catalyst deactivation.

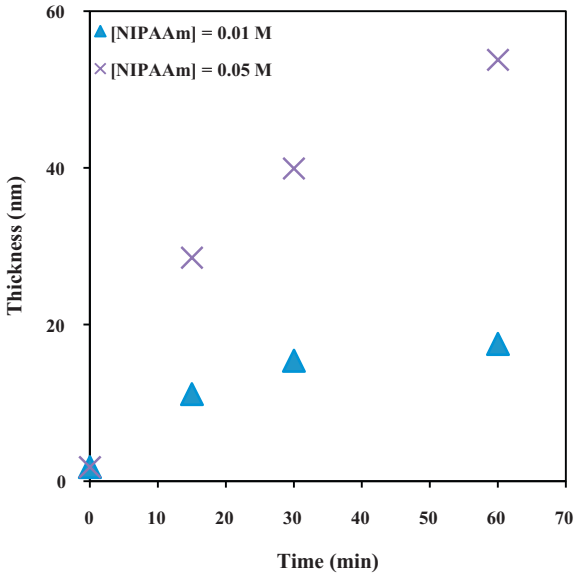

Fig. 1. Dependence of dry polymer layer thickness on polymerization time for surface-initiated ATRP of PNIPAAm from initiator-functionalized, PGMA-coated silicon substrates.

While well-controlled growth would improve the reinitiation efficiency of PPEGMA in block copolymer nanolayers, our results clearly show that the chains remain active for relatively long polymerization times, and, hence, it is possible to use polymerization time to adjust the PNIPAAm layer thickness and still preserve some fraction of chain ends for subsequent reinitiation. Significant effort was made to vary the polymerization conditions and formulation to improve control. Results are presented in the Supplemental Information. In one experiment, we used the same formulation and reaction conditions as Masci et al. [34], who reported controlled solution-phase polymerization of PNIPAAm by ATRP in a 50:50 (v/v) mixed solvent system of dimethylformamide and water at 20 °C. Using their formulation for surface-initiated ATRP of PNIPAAm failed to give controlled growth. It is not completely surprising to see such differences between solution-phase and surface-initiated ATRP, since higher chain density on the surface leads to higher probability for chain termination [35].

Surface topography and roughness of the silicon substrates before and after modification were determined by AFM. Fig. 2 shows representative 1 μm × 1 μm topographical images of the unmodified and PNIPAAm-modified silicon surface. The RMS roughness value increased from 0.4 nm for unmodified surfaces (Fig. 2A) to 0.6 nm for surfaces modified for 1 h with NIPAAm at concentration of 0.1 M (Fig. 2B). Tu et al. [32] fabricated patterned PNIPAAm brushes on oxidized silicon wafers by surface-initiated ATRP from a micro-patterned initiator and obtained RMS surface roughness of 2–4 nm from AFM topographical analysis. Cheng et al. [36] used plasma polymerization to surface immobilize PNIPAAm on silicon wafers and the surface RMS roughness at 25 °C was 5.3 ± 1.1 nm. Therefore, the low surface roughness values are consistent with the findings from other groups, and it appears that our ATRP protocol provides somewhat smoother surfaces than found previously.

3.2. Temperature responsiveness of PNIPAAm nanolayers on silicon substrate

Ellipsometry swelling measurements were conducted to investigate thickness responsiveness to temperature change of the PNIPAAm nanolayers grafted from the silicon substrates. AFM phase imaging was used to visualize the temperature responsiveness of these nanolayers. The measurements were done in water, such that the grafted polymer chains would be solvated. Ellipsometry data in Fig. 3 show that the PNIPAAm nanolayer responded to temperature change; the swollen polymer layer thickness decreased with increasing temperature. The LCST transition occurs over a broad temperature range (25–40 °C), yet it is known that the LCST for PNIPAAm in water occurs within ±2 °C of 32 °C [37]. This result also was observed by Tu et al. [32] who reported a broad LCST transition for surface grafted PNIPAAm over a temperature range of 20–35 °C, with the majority of the transition occurring between 28 and 32 °C. For surface grafted chains, the high grafting density leads to strong inter-chain interactions and these affect the observed LCST. Due to the strong inter-chain interactions, the observed LCST is not truly a second-order tran-

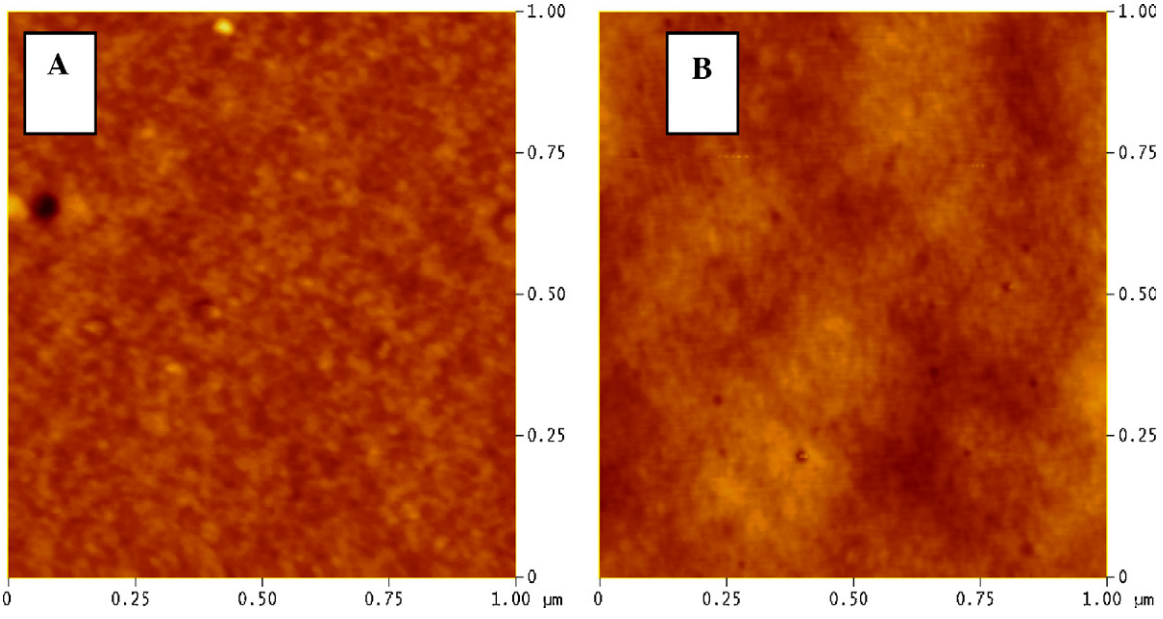

Fig. 2. AFM topographical images (1 μm × 1 μm) of PNIPAAm nanolayers on silicon substrates. (A) Unmodified surface, RMS roughness = 0.4 nm. (B) PNIPAAm-modified surface, RMS roughness = 0.6 nm.

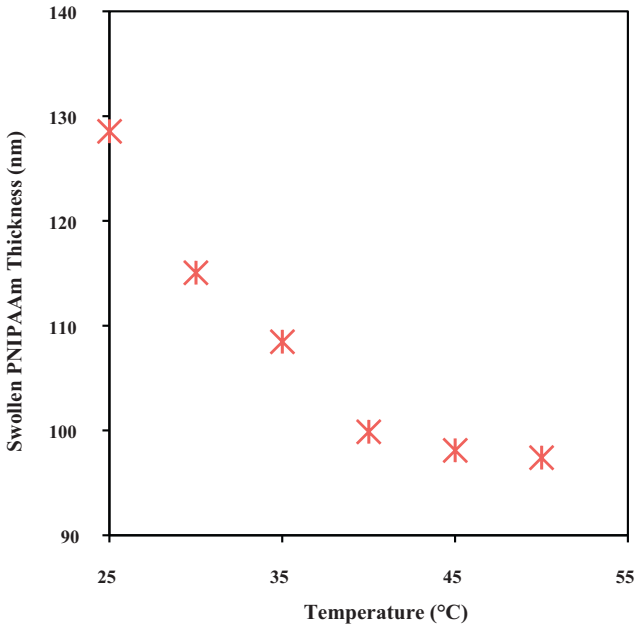

Fig. 3. Dependence of swollen PNIPAAm layer thinkness on temperature. The flat silicon surface had a dry layer polymer thickness of 85.6 nm.

sition. A swelling ratio ($h_{swollen}/h_{dry}$) of 2.00 was obtained for the solvated PNIPAAm nanolayer at 25 °C. The swelling ratio decreased gradually with increasing temperature, reaching a value of 1.53 at 45 °C. Generally, moderate to low swelling ratios were obtained, which can be attributed to the high graft densities we attained on the silicon surface (vide infra).

Fig. 4 shows AFM phase images (1 μm × 1 μm) of a solvated PNIPAAm nanolayer at temperatures above and below LCST. The phase image at 25 °C (Fig. 4A) shows fully formed globules on the surface, while the phase image at 45 °C (Fig. 4B) shows that the globules have collapsed to form a flat surface. This result illustrates 'visually' that the modified silicon surfaces responded to the temperature change.

Swelling measurements also provided data that we needed to estimate the degree of polymerization, N, and the grafting density, σ, of the grafted PNIPAAm chains. Eq. (2) was used to estimate N. This equation is based on work presented by Milner and coworkers [38,39], who conducted a self-consistent mean field (SCF) analysis of a grafted polymer brush and developed an analytical expression for swollen polymer brush thickness:

$$N = \frac{2.303(h_{swollen})^{3/2}}{(h_{dry})^{1/2}} \quad (2)$$

The constant in Eq. (2) depends on the value of the excluded volume parameter and the Kuhn length for a monomer unit. We used values of 1.2 and 8.1 Å for these parameters in PNIPAAm [40]. The $h_{swollen}$ value predicted by SCF analysis results from a parabolic density profile, while the thicknesses collected from the ellipsometry data (h_{ellip}) use an Alexander-deGennes (box-like) model. To correct this discrepancy, we utilized the adjustment proposed by Samadi et al. [31], where the h_{ellip} values measured by ellipsometry were multiplied by 4/3 for our calculation of N. Table 2 presents the results.

The grafting density was calculated by Eq. (3):

$$\sigma = \frac{\rho_o h_{dry} N_A}{m_o N} \quad (3)$$

The dry layer density, ρ_o, was assumed to be equal to the bulk density of PNIPAAm (1.103 g/cm^3) [41]. m_o is the monomer molecular weight, and N_A is Avogadro's number. Results obtained from Eqs. (2) and (3) enabled us to calculate the distance between grafting sites, d, and the radius of gyration, R_g, which provided us with an insight on the solvated PNIPAAm chain configuration. Chain-to-chain distance, d, was calculated using Eq. (4), assuming that the chains occupy a cylindrical volume normal to the surface; while the R_g of the PNIPAAm chains in water was calculated using Eq. (5) [42]:

$$d = \left[\frac{4}{\pi\sigma}\right]^{1/2} \quad (4)$$

$$R_g = 3.315(N)^{0.5} \quad (5)$$

Table 2 summarizes the results obtained for the same PNIPAAm-modified silicon substrate in water. The silicon substrate had a PNIPAAm dry layer thickness of 85.6 nm. Moderate to low swelling ratios were obtained, which can be attributed to the high graft densities on the silicon substrates. With such high graft densities, the PNIPAAm chains adopted a stretched configuration in the dry state. As a consequence, placing them in water does not induce a significant change chain length. Similar values of grafting density and swelling ratios were found by Samadi et al. [31] for graft polymerization of polystyrene from PGMA-coated silicon substrates. By comparison, the estimated grafting density of 0.09 chains/nm^2 on the silicon substrate is similar to the value of 0.17 chains/nm^2 on regenerated cellulose macroporous membranes estimated in recent work by our group [43]. While the nature of the polymer is different in these two studies, the close comparison in estimated grafting densities gives us confidence that the PGMA-coated silicon serves as a good model substrate.

Stretched polymer chain configurations are characterized by $d < 2R_g$. Table 2 shows that our calculated d value was significantly less than $2R_g$. The high graft density on the silicon surface prevents the PNIPAAm chains from collapsing to the dimension that they would adopt in free solution at 45 °C (above LCST). This result is important for design considerations since the function of the PNIPAAm layer is to swell during the rinse step to facilitate the removal of accumulated foulants. Increasing the degree of swelling may be accomplished by decreasing the grafting density [44], and we will explore this idea fully in a future publication.

3.3. Membrane modification and characterization

PNIPAAm-*b*-PPEGMA was grafted from regenerated cellulose (RC) ultrafiltration membranes using surface-initiated ATRP. The ATR-FTIR spectra in Fig. 5 confirmed the successful grafting of both polymers from the membrane surfaces. Spectrum A (bottom) represents the unmodified membrane, spectrum B (middle) represents the PNIPAAm-modified membrane, and spectrum C (top) represents the PNIPAAm-*b*-PPEGMA-modified membrane. Following polymerization, increases in intensity of peaks at 1630 and 1580 cm^{-1} are characteristic of amide carbonyl groups and N–H bending of PNIPAAm. Peaks in the range 1366–1466 cm^{-1} also increased and these are assigned to symmetrical and asymmetrical deformation bands associated with the isopropyl group in PNIPAAm. A peak at 1710 cm^{-1} is attributed to the carbonyl group in the methacrylate backbone of PPEGMA.

Atomic force microscopy was carried out to characterize the changes in the surface topography and roughness of the membranes before and after modification. Fig. 6 shows representative topographical images (1 μm × 1 μm) of the unmodified (Fig. 6A) and PNIPAAm-*b*-PPEGMA-modified (Fig. 6B) membrane surfaces. The images show only minor topographical differences between the unmodified and modified membrane surfaces. Root mean square (RMS) roughness decreased from 2.6 nm for the unmodified membrane to 2.5 nm for the PNIPAAm-modified membrane and

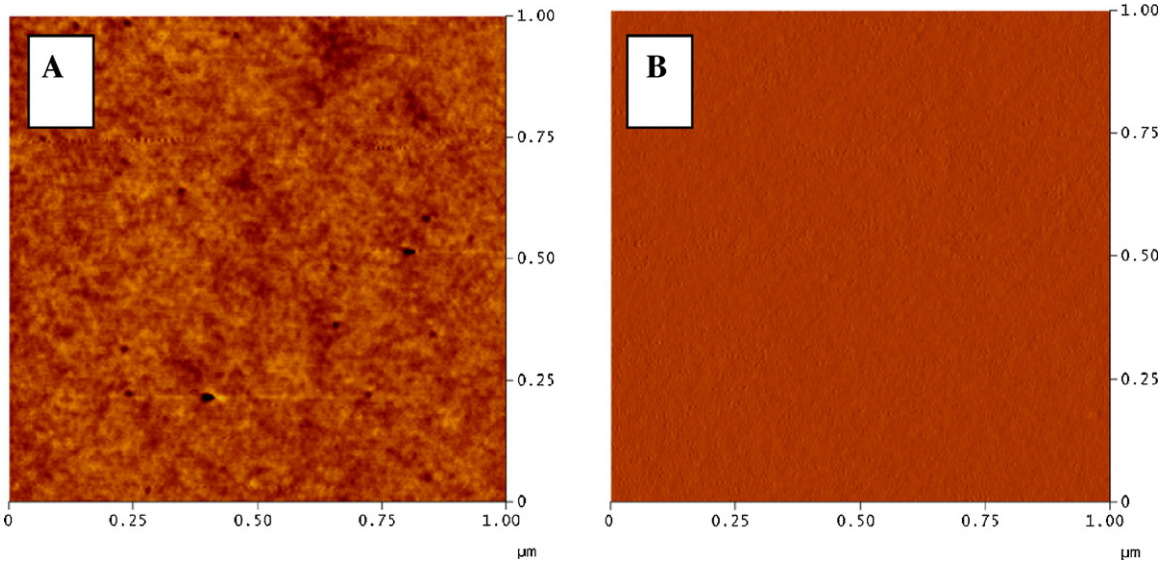

Fig. 4. AFM phase images (1 μm × 1 μm) of PNIPAAm-modified silicon surface in water at 25 °C (A) and at 45 °C (B).

Table 2
Swelling experiment results for PNIPAAm nanolayers grafted from silicon substrates.

Temperature (°C)	h_{dry} (nm)	h_{ellip} (nm)	$h_{swollen}$ (nm)	N	R_g (nm)	σ (chains/nm^2)	d (nm)	Swelling ratio
25	85.6	128.6	171.4	5600	25	0.090	3.8	2.00
30	85.6	115.1	153.4					1.79
35	85.6	108.5	144.6					1.69
40	85.6	99.9	133.2					1.56
45	85.6	98.1	130.8					1.53
50	85.6	97.4	129.9					1.52

to 1.7 nm for the PNIPAAm-*b*-PPEGMA-modified membrane. Our group previously has observed decreased surface roughness following modification of microporous membranes by ATRP [21,24]. Other groups also have reported that surface-initiated polymerization tends to make rougher surfaces smoother [45,46]. This observation is particularly important since earlier studies have shown that decreasing surface roughness leads to less adsorption of organic compounds and, hence, decreases surface fouling [1]. Results have shown that colloidal fouling of reverse osmosis and nanofiltration membranes is correlated nearly perfectly with membrane surface roughness in all cases, regardless of physical and chemical operating conditions. Colloidal particles (foulants) accumulate preferentially in valleys of relatively open and rough membrane surfaces causing valley clogging and increasing resistance to water transport [47].

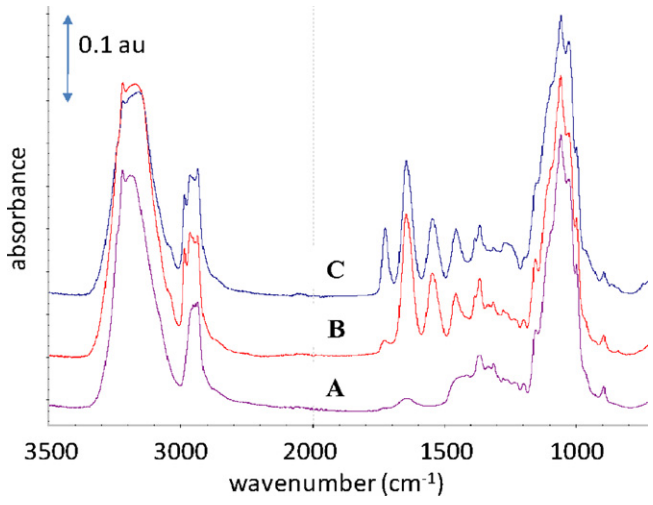

Fig. 5. ATR-FTIR spectra for (A, bottom) unmodified regenerated cellulose UF membrane, (B, middle) membrane following modification with NIPAAm at concentration of 0.1 M for 1 h, and (C, top) membrane following modification with NIPAAm at concentration of 0.1 M for 1 h followed by modification with PEGMA at concentration of 0.1 M for 3 h.

3.4. Membrane performance

Performance of the surface-modified membranes was evaluated by carrying out permeate flux experiments using synthetic produced water. The reason to use synthetic PW was to ensure constant properties that allow repeatable testing of membranes. Many possibilities exist for developing an artificial PW. Our solution was developed to have representative values for oil content, conductivity and TDS. Having said that, the properties of produced water vary and depend on the geography, geological formation, and type of hydrocarbon produced by the field (oil production, coal bed methane production). PW properties also may change during the lifetime of the reservoir. Components may include dispersed oil, soluble organics (PAHs, phenols, organic acids, etc.), treatment chemicals (corrosion inhibitors, scale inhibitors, biocides, emulsion breakers, etc.), carbonate and sulfate salts, silicates, bacteria, metals, etc. The USGS has established a database of analyzed PWs [48].

Synthetic produced water composed of soybean oil, NaCl and water was used to measure the flux of the unmodified and surface-modified RC UF membranes at 207 kPa. Fig. 7 shows data on flux versus filtration time for unmodified, PNIPAAm-modified and PNIPAAm-*b*-PPEGMA-modified membranes. To study how effective cold DI water was at detaching any foulants that had accumulated on the membrane surface during the first filtration run,

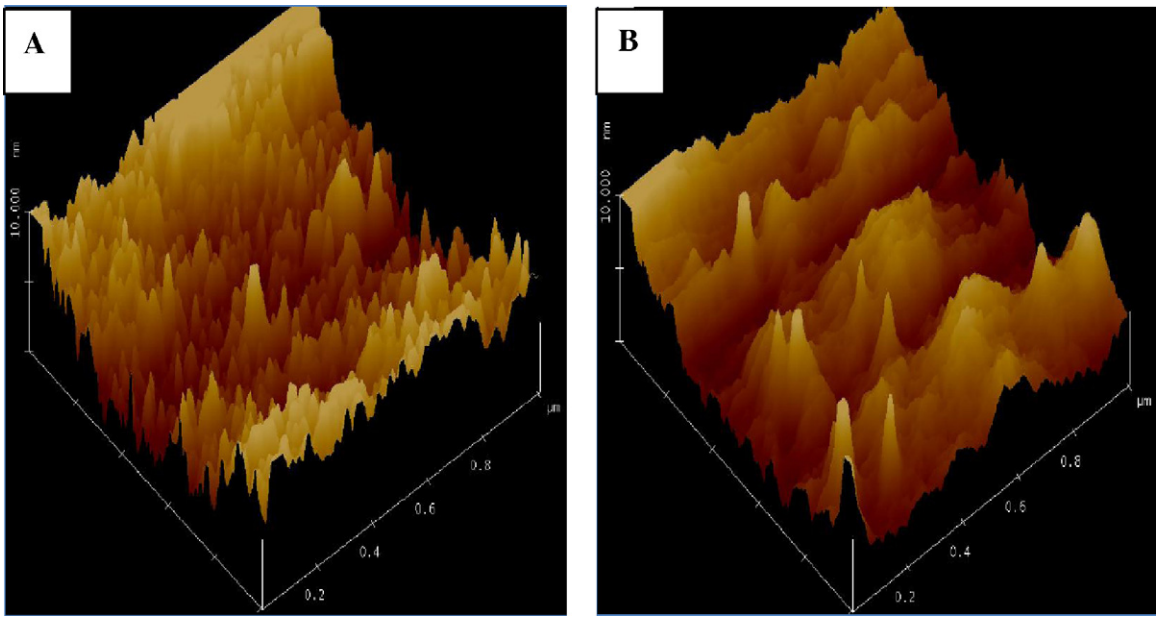

Fig. 6. AFM topographical dry layer images (1 μm × 1 μm) of membrane surfaces. (A) Unmodified regenerated cellulose 5 kDa UF membrane, RMS roughness = 2.6 nm. (B) PNIPAAm-*b*-PPEGMA-modified membrane, RMS roughness = 1.7 nm.

a second warm (45 °C) produced water filtration run was carried out after a cold (15 °C) DI water rinse. This enabled us to calculate the flux recovery that was attainable by a simple water rinse. The grafted temperature-responsive block (PNIPAAm) swells and becomes hydrophilic in cold water below LCST (around 32 °C). We expect foulants attached to the surface at temperatures above 32 °C to detach during the cold water rinse (below 32 °C) as a result of this phase change. This rinse should provide more effective flux recovery for the modified membranes than unmodified membranes.

Polymer grafting from the membranes led to decreases in the water flux; the flux decreased by 38% after PNIPAAm modification and by 40% after PNIPAAm-*b*-PPEGMA modification. This demonstrates that polymer grafting from the membrane surface provides an additional resistance to flow. Given that the estimated nanolayer thickness is much larger than the average effective pore size of the membrane, a dense polymer nanolayer forms at the membrane surface. Thus, it may be possible to minimize the decrease in water flux by changing the nanolayer thickness and chain density. Nevertheless, the final flux was comparable to those of commercial membranes used for removal of organics with high salt passage (e.g., GE Septa™, GE Osmonics; Liqui-Flux®, Membrana GmbH).

The long-term performance characteristics of the surface-modified membranes were evaluated by carrying out cross-flow filtration experiments using our model synthetic PW. Fig. 8 shows

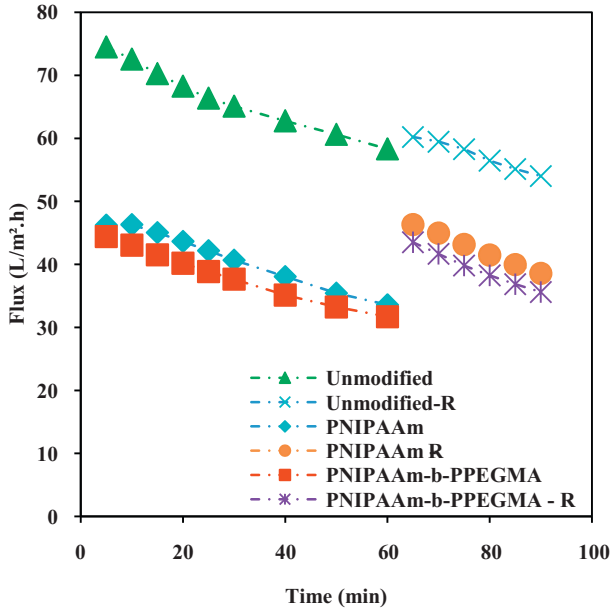

Fig. 7. Synthetic produced water flux measurements by dead-end filtration for unmodified, PNIPAAm-modified and PNIPAAm-*b*-PPEGMA-modified RC 5 kDa UF membranes. A second filtration run was carried out for each of these membranes after a cold water (15 °C) rinse, indicated by the letter R in the legend. A constant pressure of 207 kPa was used for all of the experiments.

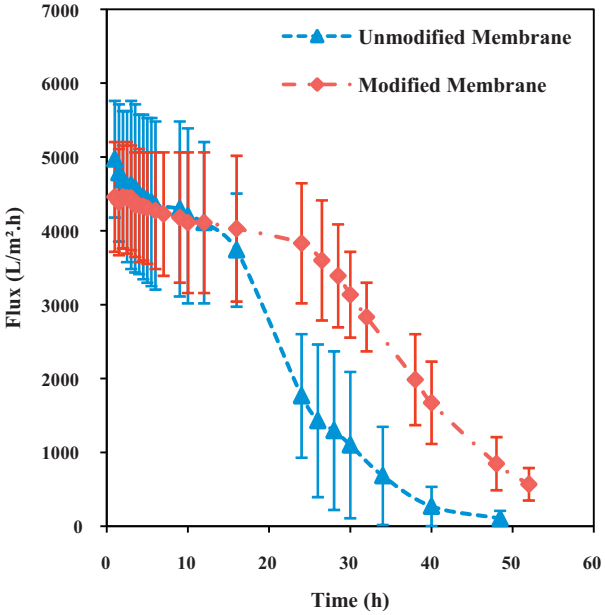

Fig. 8. Synthetic produced water flux measurements by cross-flow filtration using unmodified and PNIPAAm-*b*-PPEGMA-modified RC 1000 kDa UF membranes. Experiments were carried out at a temperature of 50 °C and a TMP of 414 kPa. Symbols represent average values for two runs using different membranes. Error bars indicate the standard error.

Table 3
Permeate quality after filtration of synthetic produced water using unmodified, PNIPAAm-modified and PNIPAAm-*b*-PPEGMA-modified RC 5 kDa membranes.

Membrane	Conductivity (μS/cm)	TDS (mg/L)	TOC (mg/L)	TOC removal (%)
Unmodified	1038	508	4.91	94.02
PNIPAAm	1024	502	3.30	95.99
PNIPAAm-*b*-PPEGMA	1021	500	2.02	97.54

synthetic PW flux measurements (permeate flux versus time) by cross-flow filtration for unmodified and PNIPAAm-*b*-PPEGMA-modified RC 1000 kDa UF membranes. Symbols represent average values measured for two runs using two different membranes. All experiments were carried out at a temperature of 50 °C and a TMP of 414 kPa. Not surprisingly, permeate flux at the start of the experiment was lower for the modified membrane than for the unmodified membrane. However, the modified membrane experienced a slower rate of flux decline than the unmodified membrane, and, as a result, the instantaneous fluxes of both membranes were equal after 12 h. Permeate fluxes through both membranes continued to decline, but, after this cross-over point, permeate flux through the modified membrane always exceeded flux through the unmodified membrane. The total volume of permeate processed through modified membrane was 13.8% more than the total permeate that was processed through the unmodified membrane after 40 h of operation. Clearly, the modified membrane allowed higher cumulative volumes of water to be processed over time prior to cleaning. This same observation was made by Louie et al. [49] in their work on physical coating of reverse osmosis membranes with a polyether–polyamide block copolymer (PEBAX®). They reported that despite the significant flux loss observed post modification, the modified membranes showed slower flux decline over time and allowed for higher cumulative volumes of water to be processed. Percentage flux decline for the block copolymer nanolayer is lower than the PNIPAAm layer alone. When carrying out warm (45 °C) water filtration runs, we expect the PNIPAAm to collapse and become hydrophobic; thus, PPEGMA, which is the upper block, is important for suppression of foulant attachment during filtration.

Our results also showed that the flux recovery was better for the modified membranes after a cold water rinse. The flux recovered fully to initial values for both the PNIPAAm- and PNIPAAm-*b*-PPEGMA-modified membranes; while only ~81% of the initial flux was recovered for the unmodified membrane. Control experiments with a warm water rinse (above LCST for PNIPAAm) yielded lower flux recoveries than results with the cold water rinse. The high flux recovery for the unmodified membranes was not surprising since the regenerated cellulose layer is hydrophilic and resistant to irreversible fouling. It also should be noted from our AFM measurements that all three membranes had low surface roughness, a characteristic that should lead to less adsorption of organic foulants.

Table 3 shows results of the permeate quality measurements after filtration of our synthetic produced water using unmodified, PNIPAAm-modified and PNIPAAm-*b*-PPEGMA-modified RC 5 kDa membranes. All three membranes yielded poor salt rejection as indicated by the high permeate conductivity and TDS concentrations. Ultrafiltration membranes are not used for salt rejection in water treatment applications, and, as we discovered, even reducing the average effective pore size through membrane surface modification did not improve their salt rejection. TOC removal was high; removal efficiencies were higher than 94% for all the three membranes. The significance of the differences in the TOC removal efficiencies of the unmodified and modified membranes was relatively small.

4. Conclusions

We have demonstrated that by grafting PNIPAAm-*b*-PPEGMA nanolayers from regenerated cellulose membranes we can change the membrane surface properties in ways that limit foulant accumulation on these membranes and provide an easy, chemical-free way to remove any attached foulants. The dual functionality provided by this block copolymer system yields fouling-resistant and temperature-responsive membranes for the treatment of oily water.

Surface-initiated polymerization of PNIPAAm from silicon substrates that were designed to mimic a polymeric membrane surface showed that PNIPAAm chains remain active for relatively long polymerization times, and, hence, it is possible to use polymerization time to adjust the nanolayer thickness and still preserve some fraction of chain ends for subsequent reinitiation. These studies also demonstrated the responsive nature of the PNIPAAm nanolayers and quantified the degree of layer swelling for grafted PNIPAAm.

PNIPAAm-*b*-PPEGMA was grafted by surface-initiated ATRP from regenerated cellulose UF membranes. ATR-FTIR spectra confirmed the successful grafting of both polymers from the membrane surface. From AFM topographical images, we observed that the membrane surface roughness decreased following PNIPAAm-*b*-PPEGMA modification.

Polymer grafting led to decreases in the water flux but the modified membranes showed slower flux decline over time. The modified membranes allowed higher cumulative volumes of water to be processed over time prior to cleaning. Flux recovery was better for the modified membranes after a cold water rinse. Modified membranes achieved 100% flux recovery, while only ~81% of the initial flux was recovered for the unmodified membrane. TOC removal efficiencies were higher than 94% for all the three membranes studied and increased slightly with increasing degree of modification. However, all the three membranes exhibited poor salt rejection, indicating that a polishing step such as reverse osmosis would be needed to recover the water for beneficial use. The modification strategy can be transferred easily to other membrane support materials where irreversible fouling may be more detrimental to performance than we have found for regenerated cellulose membranes.

Acknowledgement

The authors thank the National Science Foundation for support under award CBET 0651646.

Appendix A. Supplementary data

Supplementary data associated with this article can be found, in the online version, at doi:10.1016/j.memsci.2011.03.010.

References

[1] S. Mondal, S.R. Wickramasinghe, Produced water treatment by nanofiltration and reverse osmosis membranes, J. Membr. Sci. 322 (2008) 162–170.
[2] C.E. Clark, J.A. Veil, Produced water volumes and management practices in the United States, prepared by the Environmental Science Division, Argonne

National Laboratory for the U.S. Department of Energy, Office of Fossil Energy, National Energy Technology Laboratory, September 2009.
[3] Z. Khatib, P. Verbeek, Water to value—produced water management for sustainable field development of mature and green fields, J. Petrol. Technol. 55 (2003) 26–28.
[4] Advanced Resources International, Powder River Basin coal bed methane development and produced water management study, prepared for the U.S. Department of Energy, National Energy Technology Laboratory, November 2002.
[5] C.A. Rice, V. Nuccio, Water produced with coal bed methane, in: USGS Fact Sheet FS, 2000, pp. 156–160.
[6] T. Hayes, D. Arthur, Overview of emerging treatment technologies, in: Proceedings of the 11th Annual International Petroleum Environmental Conference, Albuquerque NM, October 12–15, 2004.
[7] K. Keith, J. Bauder, J. Wheaton, Frequently Asked Questions, Coal Bed Methane (CBM), Montana State University-Bozeman and Montana Bureau of Mines and Geology, 2003.
[8] M Cheryan, N. Rajagopalan, Membrane processing of oily streams. Wastewater treatment and waste reduction, J. Membr. Sci. 151 (1998) 13–28.
[9] P. Xu, J.E. Drewes, Viability of nanofiltration and ultra-low pressure reverse osmosis membranes for multi-beneficial use of methane produced water, Sep. Purif. Technol. 52 (2006) 67–76.
[10] P. Xu, J.E. Drewes, D. Heil, Beneficial use of co-produced water through membrane treatment: technical-economic assessment, Desalination 225 (2008) 139–155.
[11] A. Asatekin, A.M. Mayes, Oil industry wastewater treatment with fouling resistant membranes containing amphiphilic comb copolymers, Environ. Sci. Technol. 43 (2009) 4487–4492.
[12] A.C. Sagle, E.M. Van Wagner, H. Ju, B.D. McCloskey, B.D. Freeman, M.M. Sharma, PEG-coated reverse osmosis membranes: desalination properties and fouling resistance, J. Membr. Sci. 340 (2009) 92–108.
[13] A. Szep, R. Kohlheb, Water treatment technology for produced water, Water Sci. Technol. 62 (2010) 2372–2380.
[14] J. Mueller, Y. Cen, R.H. Davis, Cross flow microfiltration of oily water, J. Membr. Sci. 129 (1997) 221–235.
[15] N. Hilal, O.O. Ogunbiyi, N.J. Miles, R. Nigmatullin, Methods employed for control of fouling in MF and UF membranes: a comprehensive review, Sep. Sci. Technol. 40 (2005) 1957–2005.
[16] N. Singh, Z. Chen, N. Tomer, S.R. Wickramasinghe, N. Soice, S.M. Husson, Modification of regenerated cellulose ultrafiltration membranes by surface-initiated atom transfer radical polymerization, J. Membr. Sci. 311 (2008) 225–234.
[17] K. Matyjaszewski, P.J. Miller, N. Shukla, B. Immaraporn, A. Gelman, B.B. Luokala, T.M. Siclovan, G. Kickelbick, T. Vallant, H. Hoffmann, T. Pakula, Polymers at interfaces: using atom transfer radical polymerization in the controlled growth of homopolymers and block copolymers from silicon surfaces in the absence of untethered sacrificial initiator, Macromolecules 32 (1999) 8716–8724.
[18] J. Kim, W. Huang, M.L. Bruening, G.L. Baker, Synthesis of triblock copolymer brushes by surface-initiated atom transfer radical polymerization, Macromolecules 35 (2002) 5410–5416.
[19] A. Friebe, M. Ulbricht, Cylindrical pores responding to two different stimuli via surface-initiated atom transfer radical polymerization for synthesis of grafted diblock copolymers, Macromolecules 42 (2009) 1838–1848.
[20] E. Berndt, M. Ulbricht, Synthesis of block copolymers for surface functionalization with stimuli-responsive macromolecules, Polymer 50 (2009) 5181–5191.
[21] B.V. Bhut, S.R. Wickramasinghe, S.M. Husson, Preparation of high-capacity, weak anion-exchange membranes for protein separations using surface-initiated atom transfer radical polymerization, J. Membr. Sci. 325 (2008) 176–183.
[22] N. Tomer, S. Mondal, D. Wandera, S.R. Wickramasinghe, S.M. Husson, Modification of nanofiltration membranes by surface-initiated atom transfer radical polymerization for produced water filtration, Sep. Sci. Technol. 44 (2009) 3346–3368.
[23] B.V. Bhut, S.M. Husson, Dramatic performance improvement of weak anion-exchange membranes for chromatographic bioseparations, J. Membr. Sci. 337 (2009) 215–223.
[24] N. Singh, S.M. Husson, B. Zdyrko, I. Luzinov, Surface modification of microporous PVDF membranes by ATRP, J. Membr. Sci. 262 (2005) 81–90.
[25] N. Singh, J. Wang, M. Ulbricht, S.R. Wickramasinghe, S.M. Husson, Surface-initiated atom transfer radical polymerization: a new method for preparation of polymeric membrane adsorbers, J. Membr. Sci. 309 (2008) 64–72.
[26] M. Balachandra, G.L. Baker, M.L. Bruening, Preparation of composite membranes by atom transfer radical polymerization initiated from a porous support, J. Membr. Sci. 227 (2003) 1–14.
[27] L. Sun, J. Dai, G.L. Baker, M.L. Bruening, High-capacity, protein binding membranes based on polymer brushes grown in porous substrates, Chem. Mater. 18 (2006) 4033–4039.
[28] A. Friebe, M. Ulbricht, Controlled pore functionalization of poly(ethylene terephthalate) track-etched membranes via surface-initiated atom transfer radical polymerization, Langmuir 23 (2007) 10316–10322.
[29] M. Heskins, J.E. Guillet, Solution properties of poly(N-isopropylacrylamide), J. Macromol. Sci. Chem. 8 (1968) 1441–1455.
[30] D. Wandera, S.R. Wickramasinghe, S.M. Husson, Stimuli-responsive membranes, J. Membr. Sci. 357 (2010) 6–35.
[31] S.M. Samadi, Y. Husson, I. Liu, S.M. Luzinov, I.I. Kilbey, Low temperature growth of thick polystyrene brushes via ATRP, Macromol. Rapid Commun. 26 (2005) 1829–1834.
[32] H. Tu, C.E. Heitzman, P.V. Braun, Patterned poly(N-isopropylacrylamide) brushes on silica surfaces by microcontact printing followed by surface-initiated polymerization, Langmuir 20 (2004) 8313–8320.
[33] T. Karanfil, I. Erdogan, M.A. Schlautman, Selecting filter membranes for measuring DOC and UV_{254}, J. Am. Water Works Assoc. 95 (2003) 86–100.
[34] G. Masci, L. Giacomelli, V. Crescenzi, Atom transfer radical polymerization of N-isopropylacrylamide, Macromol. Rapid Commun. 25 (2004) 559–564.
[35] J. Kim, W. Huang, M.D. Miller, G.L. Baker, M.L. Bruening, Kinetics of surface-initiated atom transfer radical polymerization, J. Polym. Sci. Part A: Polym. Chem. 41 (2003) 386–394.
[36] X. Cheng, H.E. Canavan, M.J. Stein, J.R. Hull, S.J. Kweskin, M.S. Wagner, G.A. Somorjai, D.G. Castner, B.D. Ratner, Surface chemical and mechanical properties of plasma-polymerized N-isopropylacrylamide, Langmuir 21 (2005) 7833–7841.
[37] H.G. Schild, Poly(N-isopropylacrylamide): experiment, theory and application, Prog. Polym. Sci. 17 (1992) 163–249.
[38] S.T. Milner, Compressing polymer "brushes": a quantitative comparison of theory and experiment, Europhys. Lett. 7 (1988) 695–699.
[39] S.T. Milner, T.A. Witten, M.E. Cates, Theory of the grafted polymer brush, Macromolecules 21 (1988) 2610–2619.
[40] T. Norisuye, N. Masui, Y. Kida, D. Ikuta, E. Kokufuta, S. Ito, S. Panyukov, M. Shibayama, Small angle neutron scattering studies on structural inhomogeneities in polymer gels: irradiation cross-linked gels vs chemically cross-linked gels, Polymer 43 (2002) 5289–5297.
[41] S. Burkert, E. Bittrich, M. Kuntzsch, M. Muller, K. Eichhorn, C. Bellmann, P. Uhlmann, M. Stamm, Protein resistance of PNIPAAm brushes: application to switchable protein adsorption, Langmuir 26 (2010) 1786–1795.
[42] E. Turan, S. Demirci, T. Caykara, Synthesis of thermoresponsive poly(N-isopropylacrylamide) brush on silicon wafer via atom transfer radical polymerization, Thin Solid Films 518 (2010) 5950–5954.
[43] A.R. Carter, Preparation of strong anion-exchange membranes for protein purification using atom transfer radical polymerization, Honors Thesis, Clemson University, Clemson, SC, 2010.
[44] M. Biesalski, J. Ruhe, Scaling laws for the swelling of neutral and charged polymer brushes in good solvents, Macromolecules 35 (2002) 499–507.
[45] W. Yoshida, Y. Cohen, Topological AFM characterization of graft polymerized silica membranes, J. Membr. Sci. 215 (2003) 249–264.
[46] M. Khayet, Membrane surface modification and characterization by X-ray photoelectron spectroscopy, atomic force microscopy and contact angle measurements, Appl. Surf. Sci. 238 (2004) 269–272.
[47] E.M. Vrijenhoek, S. Hong, M. Elimelech, Influence of membrane surface properties on initial rate of colloidal fouling of reverse osmosis and nanofiltration membranes, J. Membr. Sci. 188 (2001) 115–128.
[48] USGS, Produced water database, http://energy.cr.usgs.gov/prov/prodwat/index.htm (accessed December 2010).
[49] J.S. Louie, I. Pinnau, I. Ciobanu, K.P. Ishida, A. Ng, M. Reinhard, Effects of polyether–polyamide block copolymer coating on performance and fouling of reverse osmosis membranes, J. Membr. Sci. 280 (2006) 762–770.